

Closed-loop control of the position of a single vortex relative to an actuated cylinder

Daniel F. Gomez¹, Derek A. Paley¹

Abstract—We analyze a nonlinear control system consisting of a single vortex in a freestream near an actuated cylinder. We use heaving and/or surging of the cylinder as input to stabilize the vortex position relative to the cylinder. The open-loop system has two main modes of behavior based on the values of the free vortex strength and the cylinder circulation. The first mode has a single saddle point near the cylinder and, for a larger value of the cylinder circulation, the second mode has two saddle points and one center. The closed-loop system utilizes a linear state-feedback control law. We derive conditions on the control gains to stabilize any of the equilibrium points. Simulations of the open- and closed-loop systems illustrate the bifurcations that arise from varying the vortex strength, cylinder circulation and/or control gains.

I. INTRODUCTION

The creation and shedding of vortices is of importance in unsteady fluid dynamics and plays a vital role in flapping wings [1], swimming fish [2], and airfoils at high angles of attack [3]. These phenomena are very hard to model because the Navier Stokes equations with viscous effects rarely have analytical solutions and often require intensive computational power to solve to a reasonable degree of accuracy [4]. A common simplification is to use an inviscid point vortex model [5]. This model assumes that the flow is irrotational except for the vortex points and thus the flow field may be fully described using a potential function. In this formulation, the vortex dynamics are Hamiltonian and easier to work with analytically [6]. The point-vortex model is also convenient from a controls perspective since the flow can be completely described using vortex positions as states [7].

Control of vortex positions may improve lift in situations with low Reynolds number [8]. For example, the control of vortex positions is an important mechanism for insect flight and, possibly, for micro aerial vehicles [9]. The problem of stabilizing vortex positions near an airfoil has been studied using various methods such as blowing and suction from the surface of the body [10], modifying the airfoil shape to trap the vortex passively [11], and controlling the circulation around the airfoil [12].

We are interested in the stabilization of a leading edge vortex (LEV), which forms and sheds off of airfoils at high angles of attack during dynamic maneuvers. The leading edge vortex presents itself as a large vortical structure above

the airfoil that grows, sheds, and grows again [9]. Motion of the airfoil perpendicular and parallel to the freestream is called heaving and surging, respectively. We consider heaving and/or surging as control inputs to the LEV stabilization problem.

This paper presents a first step in developing a feedback control law that stabilizes a vortex near an airfoil. We model the vortical structure as a single vortex, an approach that was considered in [13], and use a cylinder instead of an airfoil, since the cylinder has a symmetric structure that eases analytic study. The cylinder and airfoil geometries are related through a conformal mapping such as the Joukowski transform and by restricting the circulation to a specific value that allows the flow to leave smoothly at the trailing edge [5].

Linearization around an equilibrium point of the system enables the design of a linear state-feedback controller that exponentially stabilizes the equilibrium point. The trace and determinant of the linearized closed-loop matrix determines conditions on the feedback gains that yield the desired behavior. Varying the feedback gains also induces bifurcations of the equilibrium points. Analyzing the local bifurcations helps understand the effect each control gain has in the global behavior of the closed-loop system.

The contributions of this paper are (1) the design of a state-feedback control for a surging and/or heaving cylinder that exponentially stabilizes any of the equilibrium points of the system; and (2) the corresponding analysis of local bifurcations that arise under variation of the closed-loop control gains. Simulations of the open- and closed-loop system illustrate these bifurcations and the corresponding vortex trajectory.

This paper is organized as follows. Section II derives the equations of motion of a single vortex near an actuated cylinder. Section III presents the various flow topologies of the open-loop system that result from the choice of system parameters. Section IV analyzes the stability of the equilibrium points of the closed-loop system, gives conditions on the feedback gains to achieve exponential stability, and presents simulation results. Section V summarizes the paper and describes ongoing work.

II. VORTEX-CYLINDER SYSTEM IN POTENTIAL FLOW

In potential flow theory, a flow field potential is found by adding the potentials corresponding to various elementary fluid flows. Consider a cylinder of radius r_0 centered at z_0 , a vortex of strength Γ_v located at z , and a freestream velocity u_∞ , where $z, z_0, u_\infty \in \mathbb{C}$ and the real and imaginary

¹Daniel F. Gomez and Derek A. Paley are with the Department of Aerospace Engineering and the Institute for Systems Research, University of Maryland, College Park, MD 20740, USA. This research was funded in part by AFOSR Grant No. FA95501810137. D. Gomez was supported by a University of Maryland Clark Doctoral Fellowship. {dfgomez, dpaley}@umd.edu

components correspond to x and y components, respectively. The potential for the freestream flow around the cylinder consists of a uniform flow, a doublet, and a vortex placed at the center of the cylinder [5]. The strength Γ_0 of the vortex placed at the center of the cylinder (from now on referred to as the bound vorticity) is a free parameter since any value obeys the boundary conditions of the flow. Let $*$ denote complex conjugation. The flow felt by the vortex corresponds to that of the freestream around a cylinder with a bound vortex plus that of an image vortex of opposite strength placed at [14]

$$z_{im} = z_0 + \frac{r_0^2}{(z - z_0)^*}. \quad (1)$$

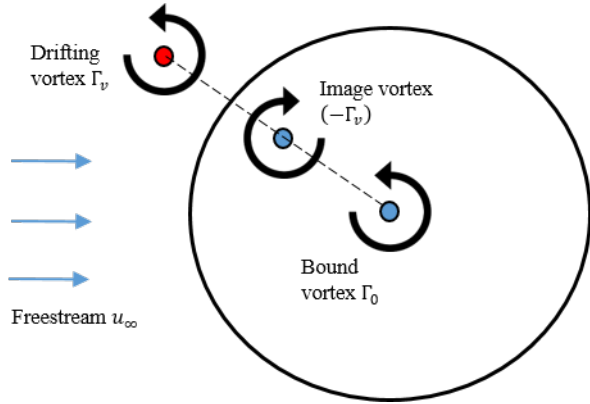


Fig. 1. The drifting vortex is convected by the influence of the freestream, the cylinder, the image vortex, and the bound vortex.

The equations of motion are derived using a complex potential. The potential $F(z)$ for a vortex placed at z , including the terms for the freestream and both image and bound vortices is

$$F(z) = u_\infty^* z + \frac{u_\infty r_0^2}{z - z_0} + \frac{\Gamma_0}{2\pi i} \log(z - z_0) - \frac{\Gamma_v}{2\pi i} \log(z - z_{im}). \quad (2)$$

The time evolution of the vortex position is given by the conjugate gradient of the potential [15], i.e.,

$$\begin{aligned} \dot{z} &= \left(\frac{dF(z)}{dz} \right)^* \\ &= u_\infty - u_\infty^* \frac{r_0^2}{((z_v - z_0)^2)^*} + \frac{i\Gamma_0}{2\pi} \frac{z_v - z_0}{|z_v - z_0|^2} \\ &\quad - \frac{i\Gamma_v}{2\pi} \frac{z_v - z_0}{|z_v - z_0|^2 - r_0^2}. \end{aligned} \quad (3)$$

To include an input term in the dynamics, assume that u_∞ consists of a nominal freestream velocity u_0 minus the input velocity due to heaving and/or surging. For simplicity of the model, ignore unsteady aerodynamic effects so the only result of heaving and/or surging is changing the effective freestream velocity. Without loss of generality, we assume that the nominal freestream is $u_0 \in \mathbb{R}, u_0 > 0$.

To simplify the algebra, normalize length and time scales so $r_0 = 1$ and $u_0 = 1$, respectively. Define

$x_1, x_2, u_1, u_2, \sigma_v, \sigma_0 \in \mathbb{R}$ such that $u_\infty = (1 - u_1 - iu_2)u_0$, $z = (x_1 + ix_2)r_0$, $\Gamma_0/2\pi = r_0 u_0 \sigma_0$, and $\Gamma_v/2\pi = r_0 u_0 \sigma_v$. x_1 and x_2 are the Cartesian coordinates of the drifting vortex, normalized by the radius of the cylinder. σ_v and σ_0 are dimensionless quantities proportional to the drifting and, respectively, bound vortex strengths. u_1 and u_2 correspond to the surging and, respectively, heaving velocity of the cylinder, normalized by the freestream velocity. In this model, the motion of the cylinder is equivalent to a change in the freestream velocity. In non-dimensional Cartesian coordinates, the equations of motion are

$$\begin{aligned} \dot{x}_1 &= \left(\frac{x_2^2 - x_1^2}{(x_1^2 + x_2^2)^2} + 1 \right) (1 - u_1) + \frac{2x_1 x_2}{(x_1^2 + x_2^2)^2} u_2 \\ &\quad - \sigma_0 \frac{x_2}{x_1^2 + x_2^2} + \sigma_v \frac{x_2}{x_1^2 + x_2^2 - 1} \\ \dot{x}_2 &= -\frac{2x_1 x_2}{(x_1^2 + x_2^2)^2} (1 - u_1) + \left(\frac{x_2^2 - x_1^2}{(x_1^2 + x_2^2)^2} - 1 \right) u_2 \\ &\quad + \sigma_0 \frac{x_1}{x_1^2 + x_2^2} - \sigma_v \frac{x_1}{x_1^2 + x_2^2 - 1}. \end{aligned} \quad (4)$$

These equations are only valid in the region $x_1^2 + x_2^2 > 1$, i.e., when the vortex is outside of the cylinder.

III. BIFURCATIONS OF THE OPEN-LOOP DYNAMICS

The location of the equilibrium points of (4) and their bifurcations are found by varying σ_0 and σ_v ; a thorough description can be found in [16]. To find the zero-input equilibrium points $(\tilde{x}_1, \tilde{x}_2)$, set $\dot{x}_1 = \dot{x}_2 = u_1 = u_2 = 0$. The equilibrium points for this system always occur along the line $\tilde{x}_1 = 0$ [16], which follows from the condition $\dot{x}_2 = 0$. Solving for $\dot{x}_1 = 0$ yields the polynomial

$$\tilde{x}_2^4 + (\sigma_v - \sigma_0)\tilde{x}_2^3 + \sigma_0\tilde{x}_2 - 1 = 0. \quad (5)$$

Depending on the value of the parameters σ_v and σ_0 , (5) can have two, three, or four real solutions. One solution always lies within the unit circle, which is not a valid equilibrium point for the system, because it is inside the cylinder. Without loss of generality, we take $\sigma_v > 0$: if $\sigma_v < 0$, we can flip the signs of σ_0, x_2 , and u_2 , i.e., reflect across the horizontal axis, and obtain the same dynamics; if $\sigma_v = 0$, the system corresponds to a free particle rather than a vortex.

With these conventions, polynomial (5) evaluated at $\tilde{x}_2 = -1$ is equal to $-\sigma_v < 0$, whereas in the limit $\tilde{x}_2 \rightarrow -\infty$, it is positive. Therefore, the polynomial must always have a root in the interval $(-\infty, -1)$. This equilibrium point exists for all values of σ_0 and σ_v and, in Section IV, we show that this point is always a saddle. In general, varying the σ_v and σ_0 will change the number of equilibrium points and their positions. Figure 2 shows the regions in parameter space for which the system has three equilibrium points: a saddle on the negative x_2 axis (the lower saddle), a saddle on the positive x_2 axis (the upper saddle), and a center on the x_2 axis between the upper saddle and the cylinder. The boundary between the regions with one and three equilibrium points corresponds to parameter values for which the system has

two equilibrium points: a saddle under the cylinder and an undefined equilibrium point above the cylinder. However, this region has zero area, is not of physical interest [16], and we ignore it in the subsequent analysis.

Figure 3 shows a bifurcation diagram varying σ_0 with fixed $\sigma_v = 2$. Fig. 4 shows trajectories in the phase plane of vortex position for $\sigma_0 = 0$: there is a single saddle below the cylinder. As σ_0 increases, the saddle point moves closer to the surface of the cylinder. At the critical value, the system exhibits a saddle-node bifurcation: a new equilibrium point appears on the opposite side of the cylinder and splits into a center and a saddle. Below the bifurcation point, the phase portrait is split into three regions: the upper region, the lower region, and periodic orbits surrounding the cylinder. Above the bifurcation point, the upper region splits into three regions, as shown in Figure 5. More phase diagram topologies for the open-loop system are described in [16].

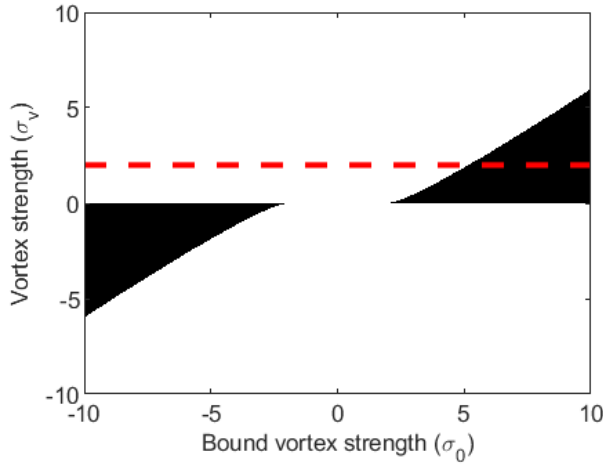


Fig. 2. The black regions show the area in parameter space where the system has three equilibrium points. The dashed line corresponds to the slice shown in Figure 3.

IV. CLOSED-LOOP CONTROL DESIGN AND ANALYSIS

In order to design a feedback controller, we linearize (4) at any one of the equilibrium points. Let (\tilde{x}, \tilde{u}) refer to evaluating the derivative at the equilibrium point $x_1 = u_1 = u_2 = 0$, $x_2 = \tilde{x}_2$. We derive the linear system

$$\begin{bmatrix} \dot{\tilde{x}}_1 \\ \dot{\tilde{x}}_2 \end{bmatrix} = A \begin{bmatrix} x_1 \\ x_2 - \tilde{x}_2 \end{bmatrix} + B \begin{bmatrix} u_1 \\ u_2 \end{bmatrix}, \quad (6)$$

where

$$A_{ij} = \left. \frac{\partial \dot{x}_i}{\partial x_j} \right|_{(\tilde{x}, \tilde{u})} \quad \text{and} \quad B_{ij} = \left. \frac{\partial \dot{x}_i}{\partial u_j} \right|_{(\tilde{x}, \tilde{u})}, \quad i, j = 1, 2. \quad (7)$$

We have

$$A = \begin{bmatrix} 0 & \frac{\sigma_0}{\tilde{x}_2^2} - \frac{\sigma_v(\tilde{x}_2^2 + 1)}{(\tilde{x}_2^2 - 1)^2} - \frac{2}{\tilde{x}_2^3} \\ \frac{\sigma_0}{\tilde{x}_2^2} - \frac{\sigma_v}{(\tilde{x}_2^2 - 1)} - \frac{2}{\tilde{x}_2^3} & 0 \end{bmatrix} \quad (8)$$

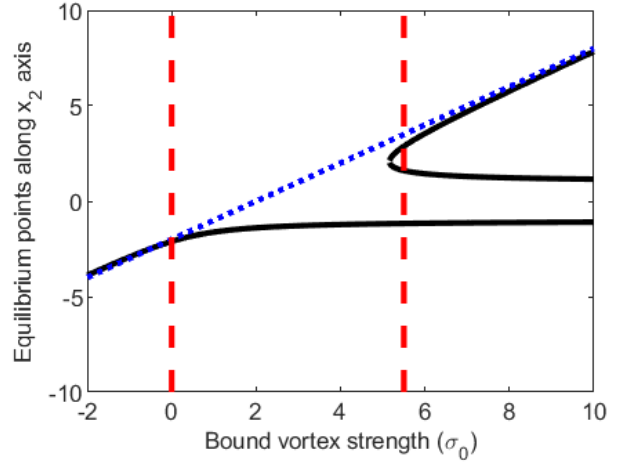


Fig. 3. Bifurcation diagram fixing $\sigma_v = 2$ and varying σ_0 . Equilibrium points far from the cylinder approach the line $\sigma_0 = \sigma_v$, shown as a dotted line.

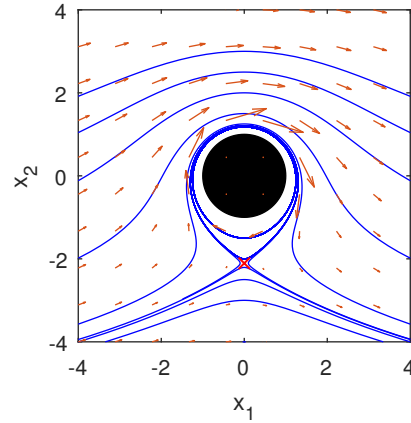


Fig. 4. Phase portrait with $\sigma_0 = 0, \sigma_v = 2$. There is a single saddle point below the cylinder. Orbits near the cylinder are periodic. Far from the cylinder, trajectories resemble the freestream.

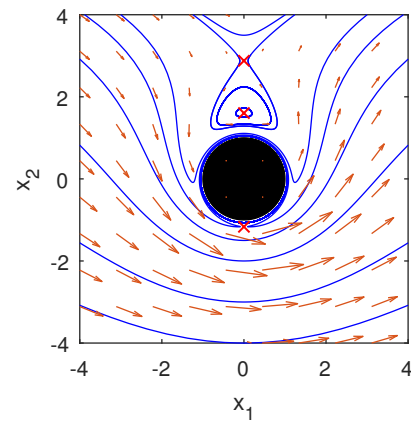


Fig. 5. Phase portrait with $\sigma_0 = 5.5, \sigma_v = 2$. There is a saddle point below the cylinder. The separatrix comes arbitrarily close to the saddle, then wraps clockwise around the cylinder getting near the saddle again, before going off to infinity.

and

$$B = \begin{bmatrix} -1 - \frac{1}{\bar{x}_2^2} & 0 \\ 0 & -1 + \frac{1}{\bar{x}_2^2} \end{bmatrix}. \quad (9)$$

Consider the linear state-feedback control

$$\mathbf{u} = \begin{bmatrix} u_1 \\ u_2 \end{bmatrix} = - \begin{bmatrix} k_{11} & k_{12} \\ k_{21} & k_{22} \end{bmatrix} \begin{bmatrix} x_1 \\ x_2 - \bar{x}_2 \end{bmatrix} = -K(\mathbf{x} - \bar{\mathbf{x}}). \quad (10)$$

The first subscript in each k indicates which control input the gain corresponds to (1 for surging and 2 for heaving) and the second subscript corresponds to which state it multiplies (x_1 or x_2). We analyze the stability of the feedback system by looking at the eigenvalues of the matrix $A - BK$, as indicated by the trace and determinant. For a 2×2 matrix, the determinant is the product of eigenvalues and the trace is the sum of eigenvalues, so the sign of the determinant and trace can be used to infer the sign of the real part of the eigenvalues and, thus, the stability properties of the system. In particular, a negative determinant implies the equilibrium point is a saddle, i.e., it has one unstable and one stable eigenvalue. If the determinant is positive, then a positive trace indicates the system is unstable and a negative trace indicates the system is exponentially stable, i.e., it is stable and will converge to the equilibrium point [17]. If the determinant is positive and the trace is 0, or if the determinant is 0, then no conclusion can be reached.

Theorem 1: For an equilibrium point \bar{x}_2 of (4) to be exponentially stable, the following two conditions need to hold:

$$k_{11}k_{22} - \left(k_{12} + \frac{1}{\bar{x}_2} - \frac{2\sigma_v\bar{x}_2^2}{(\bar{x}_2^2 - 1)^3} \right) \left(k_{21} + \frac{1}{\bar{x}_2} \right) > 0 \quad (11)$$

$$k_{11} + k_{22} + \frac{k_{11} - k_{22}}{\bar{x}_2^2} > 0. \quad (12)$$

Proof: Since (12) is the trace of $A - BK$ it must be negative for exponential stability. Condition (11) follows from requiring the determinant of $A - BK$ to be positive, i.e.,

$$\det(A - BK) = k_{11}k_{22} \frac{\bar{x}_2^4 - 1}{\bar{x}_2^4} - \left(A_{12} + \frac{\bar{x}_2^2 + 1}{\bar{x}_2^2} k_{12} \right) \left(A_{21} + \frac{\bar{x}_2^2 - 1}{\bar{x}_2^2} k_{21} \right) > 0 \quad (13)$$

$$= \left[k_{11}k_{22} - \left(\frac{A_{12}\bar{x}_2^2}{\bar{x}_2^2 + 1} + k_{12} \right) \left(\frac{A_{21}\bar{x}_2^2}{\bar{x}_2^2 - 1} + k_{21} \right) \right] \frac{\bar{x}_2^4 - 1}{\bar{x}_2^4} > 0 \quad (14)$$

$$k_{11}k_{22} - \left(\frac{A_{12}\bar{x}_2^2}{\bar{x}_2^2 + 1} + k_{12} \right) \left(\frac{A_{21}\bar{x}_2^2}{\bar{x}_2^2 - 1} + k_{21} \right) > 0. \quad (15)$$

Recall from (8),

$$A_{21} = \frac{\sigma_0}{\bar{x}_2^2} - \frac{\sigma_v}{\bar{x}_2^2 - 1} - \frac{2}{\bar{x}_2^3} \\ = \frac{\sigma_0(\bar{x}_2^3 - \bar{x}_2) - \sigma_v\bar{x}_2^3 - 2(\bar{x}_2^2 - 1)}{\bar{x}_2^3(\bar{x}_2^2 - 1)}. \quad (16)$$

Replace the term $\sigma_v\bar{x}_2^3$ from rearranging (5) as

$$\sigma_v\bar{x}_2^3 = 1 + \sigma_v(\bar{x}_2^3 - \bar{x}_2) - \bar{x}_2^4. \quad (17)$$

The terms with σ_0 cancel, leaving

$$A_{21} = \frac{\bar{x}_2^4 - 2\bar{x}_2^2 + 1}{\bar{x}_2^3(\bar{x}_2^2 - 1)} = \frac{\bar{x}_2^2 - 1}{\bar{x}_2^3}. \quad (18)$$

Notice

$$A_{12} = A_{21} - \frac{2\sigma_v}{(\bar{x}_2^2 - 1)^2}. \quad (19)$$

Finally substitute (18) and (19) into (15) to obtain (11). ■

Theorem 1 applies to any of the possible equilibrium points described in Section III. Note that with gains set to 0 and $\bar{x}_2 < 0$, the corresponding equilibrium point is a saddle, as stated in Section III. When feedback is applied, any combination of gains satisfying (11) and (12) will exponentially stabilize the desired equilibrium point. Note that the conditions (11) and (12) can be achieved using either k_{11} or k_{22} (diagonal gains) and either k_{12} or k_{21} (cross gains) while setting the other gains to zero. This corresponds to using only surging (i.e., $k_{21} = k_{22} = 0$), only heaving ($k_{11} = k_{12} = 0$), only x_1 feedback ($k_{12} = k_{22} = 0$), or only x_2 feedback ($k_{11} = k_{21} = 0$). These designs may be advantageous if there are limitations with the actuators or with the observers. Additionally, since for each design we have two gains instead of four, it is easier to analyze the effect of each gain.

Corollary 1.1: For the two-gain designs, i.e., either $k_{11} = 0$ or $k_{22} = 0$ and either $k_{12} = 0$ or $k_{21} = 0$, (11) reduces to

$$k_{12} > k_{1c} > 0 \quad \text{for the lower saddle } (\bar{x}_2 < 0) \quad (20)$$

$$k_{12} < k_{1c} > 0 \quad \text{for the center } (\bar{x}_2 > 0) \quad (21)$$

$$k_{12} < k_{1c} < 0 \quad \text{for the upper saddle } (\bar{x}_2 > 0) \quad (22)$$

or

$$k_{21} > k_{2c} > 0 \quad \text{for the lower saddle } (\bar{x}_2 < 0) \quad (23)$$

$$k_{12} > k_{2c} < 0 \quad \text{for the center } (\bar{x}_2 > 0) \quad (24)$$

$$k_{21} < k_{2c} < 0 \quad \text{for the upper saddle } (\bar{x}_2 > 0) \quad (25)$$

where

$$k_{1c} = \frac{2\sigma_v\bar{x}_2^2}{(\bar{x}_2^2 - 1)^3} - \frac{1}{\bar{x}_2}, \quad k_{2c} = -\frac{1}{\bar{x}_2}, \quad (26)$$

and (12) reduces to

$$k_{11} < 0 \quad \text{or} \quad k_{22} < 0. \quad (27)$$

Proof: In closed loop with a two-gain design and using the k_{1c} and k_{2c} as defined in (26), the stability condition (11) can be written as

$$(k_{1c} - k_{12})k_{2c} < 0 \quad \text{or} \quad k_{1c}(k_{2c} - k_{21}) < 0. \quad (28)$$

Conditions (20) to (25) are derived from (28) by isolating the corresponding gain and flipping the inequality based on the sign of k_{1c} or k_{2c} for the corresponding equilibrium point. The signs of k_{1c} or k_{2c} are determined from the position and

open-loop properties of the equilibrium points. In open-loop, the determinant condition (11) is

$$k_{1c}k_{2c} < 0. \quad (29)$$

Recall this condition holds for the center and the opposite equality holds for the saddles. For the lower saddle, $k_{1c} > 0$ and $k_{2c} > 0$, since $\tilde{x}_2 < 0$. For the center and the upper saddle, $k_{2c} < 0$ since $\tilde{x}_2 > 0$. For the center, the product $k_{1c}k_{2c} < 0$, because the equilibrium point is stable and thus $k_{1c} > 0$. Similarly, $k_{1c} < 0$ for the upper saddle, because the product $k_{1c}k_{2c} > 0$. Condition (27) follows from (12), setting either $k_{11} = 0$ or $k_{22} = 0$, and using the fact that $\tilde{x}_2^2 < 1$. ■

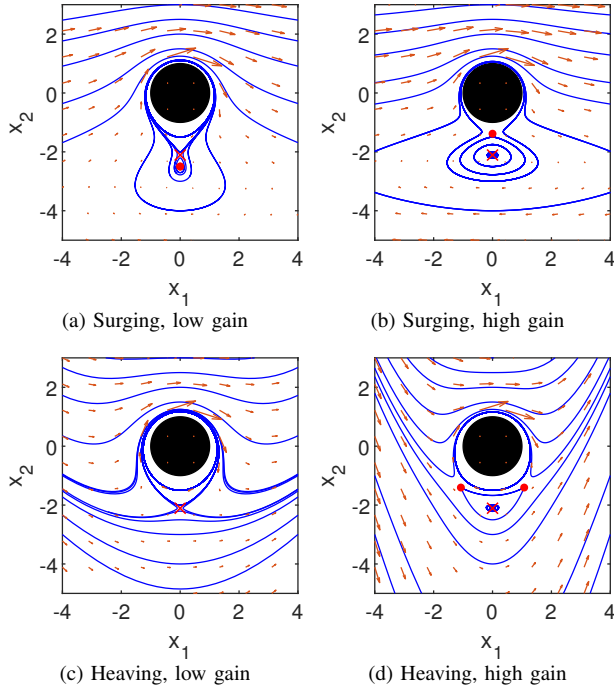


Fig. 6. Phase planes for the closed-loop system with $\sigma_v = 2, \sigma_0 = 0$, and non-zero cross gains k_{12} (a–b) or k_{21} (c–d). The red X indicates the original equilibrium point, the red dots indicate the new equilibrium points that appear due to feedback. (a) and (c) have gains below conditions (20) and (23), respectively. (b) and (d) have gains above condition (20) and (23), respectively.

Several representative cases help to visualize the behavior of the closed-loop system. Fig. 6 shows the result of using the cross gains, k_{12} or k_{21} , either 50% below or above their corresponding critical values, with all other gains set to zero. These gains need to satisfy either (20) or (23), respectively, to convert the lower saddle to a stable node or focus. In Fig. 6a, k_{12} (surging) does not satisfy (20); the original equilibrium point remains a saddle and a new stable equilibrium point appears below. This new equilibrium point requires a constant surging input, so it is equivalent to stabilizing an equilibrium point at a different nominal freestream velocity. In Fig. 6c, the heaving case, no new equilibrium points appear for low values of k_{21} . In Figs. 6b and 6d, the gains satisfy their critical conditions and, in both cases, the original equilibrium point becomes a center. In the surging case (Fig. 6b), a saddle appears between the original

equilibrium point and the cylinder, and trajectories near the original equilibrium point form clockwise periodic orbits. In the heaving case (Fig. 6b), two saddles appear and orbits near the original equilibrium point are counter-clockwise. From a physical perspective, the two new saddles that appear when choosing k_{21} to satisfy (23) can be interpreted as equilibrium points for a different angle of the nominal freestream. Note that even with a gain that satisfies the critical condition, (20) or (23), trajectories don't converge to the desired equilibrium point because the trace is zero.

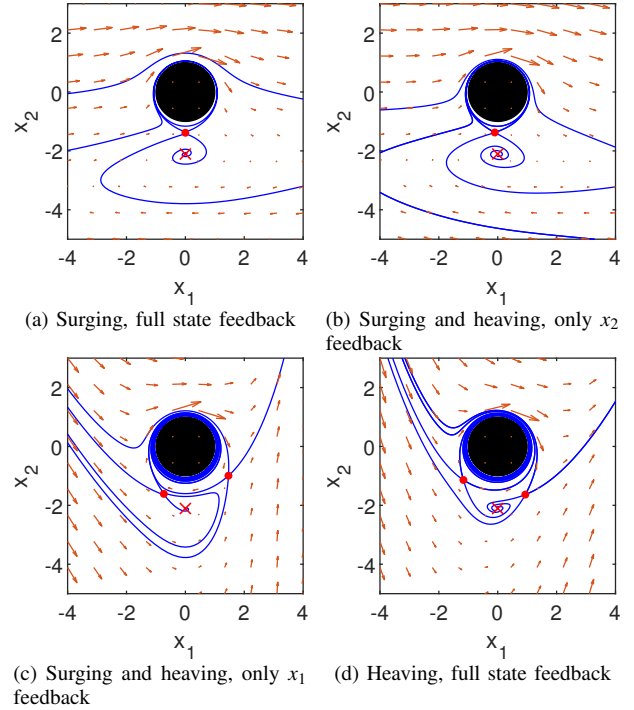


Fig. 7. Phase planes for the closed-loop with $\sigma_v = 2, \sigma_0 = 0$, and multiple two-gain designs that exponentially stabilize the equilibrium point. The red X indicates the original equilibrium point, the red dots indicate the saddles that appear due to feedback. The trajectories shown approximate the stable and unstable manifolds of the saddles.

Fig. 7 shows the effect of adding a small negative diagonal gain to the systems in Figs. 6b and 6d to make them exponentially stable. Figs. 7a and 7c have $k_{11} = -0.2$, and Figs. 7b and 7d have $k_{22} = -0.2$. The band of closed orbits surrounding the equilibrium point in Figs. 6b and 6d becomes a stable spiral that converges to the desired equilibrium point. Since the control design is based on linearization, convergence to the desired equilibrium point is only guaranteed close to the equilibrium point. We estimate the region of attraction by looking at the stable and unstable manifolds of the saddles shown in Fig. 7. These orbits separate regions in the phase plane so we can determine whether an orbit will converge by checking if it is in the same region as the stabilized equilibrium point. For the cases shown, using surging and full-state feedback results in the largest region of attraction.

V. CONCLUSION

This paper represents a first step in developing a feedback-control framework that stabilizes a vortex near an airfoil using surging and heaving as control input. Conditions on the control gains quantify the requirements to stabilize a vortex near a cylinder and guide the design of more sophisticated nonlinear controllers. The four possible gains in the linear controller are divided into two types, cross and diagonal gains, which correspond to actuation perpendicular and, respectively, parallel to the relative position of the vortex. The original saddle can be exponentially stabilized with a choice of one cross gain and one diagonal gain, while setting others to zero. The cross gains induce a saddle-center bifurcation when above a critical value. After using a cross gain to make the original equilibrium point a center, the diagonal gains exponentially stabilize the desired equilibrium point.

In ongoing work, we seek to extend these results to the case when the body is an airfoil instead of a cylinder, and is subject to physical constraints such as the Kutta condition. Preliminary analysis shows that the physical conditions that generate the open-loop bifurcations may not occur for an airfoil in quasi-steady conditions.

ACKNOWLEDGMENT

The authors thank Francis Lagor and Jonathan Lefebvre for discussions related to this project, and Travis Burch and Jordan Boehm for their feedback in preparing this paper.

REFERENCES

- [1] F. O. Minotti, "Unsteady two-dimensional theory of a flapping wing," *Physical Review E - Statistical Physics, Plasmas, Fluids, and Related Interdisciplinary Topics*, vol. 66, no. 5, p. 10, 2002.
- [2] P. Tallapragada and S. D. Kelly, "Self-propulsion of free solid bodies with internal rotors via localized singular vortex shedding in planar ideal fluids," *European Physical Journal: Special Topics*, vol. 224, no. 17-18, pp. 3185–3197, 2015.
- [3] S. Ahuja, C. Rowley, I. Kevrekidis, M. Wei, T. Colonius, and G. Tadmor, "Low-dimensional models for control of leading-edge vortices: equilibria and linearized models," *45th AIAA Aerospace Sciences Meeting and Exhibit*, pp. 1–12, 2007.
- [4] G. L. Vasconcelos, M. N. Moura, and A. M. J. Schakel, "Vortex motion around a circular cylinder," *Physics of Fluids*, vol. 23, no. 12, 2011.
- [5] J. Katz and A. Plotkin, *Low-Speed Aerodynamics*. Cambridge: Cambridge University Press, 2001.
- [6] B. N. Shashikanth, "Symmetry reduction and control of the dynamics of a 2D rigid circular cylinder and a point vortex: Vortex capture and scattering," *European Journal of Control*, vol. 13, no. 6, pp. 641–655, 2007.
- [7] B. Protas, "Vortex dynamics models in flow control problems," *Nonlinearity*, vol. 21, no. 9, pp. 202–250, 2008.
- [8] C. W. Pitt Ford and H. Babinsky, "Lift and the leading-edge vortex," *Journal of Fluid Mechanics*, vol. 720, p. 280313, 2013.
- [9] F. Manar, "Measurements and modeling of the unsteady flow around a thin wing," Ph.D. dissertation, University of Maryland, 2018.
- [10] S. I. Chernyshenko, "Stabilization of trapped vortices by alternating blowing suction," *Physics of Fluids*, vol. 7, no. 4, pp. 802–807, 1995.
- [11] V. J. Rossow, "Two-fence concept for efficient trapping of vortices on airfoils," *Journal of Aircraft*, vol. 29, no. 5, pp. 847–855, sep 1992.
- [12] Á. Péntek, J. B. Kadtko, and G. Pedrizzetti, "Dynamical control for capturing vortices near bluff bodies," *Physical Review E - Statistical Physics, Plasmas, Fluids, and Related Interdisciplinary Topics*, vol. 58, no. 2, pp. 1883–1898, 1998.
- [13] J. Kadtko, Á. Péntek, and G. Pedrizzetti, "Controlled capture of a continuous vorticity distribution," *Physics Letters A*, vol. 204, no. 2, pp. 108–114, aug 1995.
- [14] L. Milne-Thomson, *Theoretical Hydrodynamics*, ser. Dover Books on Physics. Dover Publications.
- [15] J. Roenby, "Chaos and integrability in ideal body-fluid interactions," Ph.D. dissertation, Technical University of Denmark, 2011.
- [16] J. B. Kadtko and E. A. Novikov, "Chaotic capture of vortices by a moving body. I. The single point vortex case," *Chaos (Woodbury, N.Y.)*, vol. 3, no. 4, pp. 543–553, 1993.
- [17] S. Strogatz, *Nonlinear Dynamics And Chaos*, ser. Studies in nonlinearity. Sarat Book House, 2007.